HHS Public Access

Author manuscript

J Immunol. Author manuscript; available in PMC 2020 December 01.

Published in final edited form as:

J Immunol. 2019 December 01; 203(11): 2837–2849. doi:10.4049/jimmunol.1900473.

TNF-Induced Interstitial Lung Disease in a Murine Arthritis Model: Accumulation of Activated Monocytes, Conventional Dendritic Cells, and CD21^{+}/CD23^{-} B Cell Follicles is Prevented with Anti-TNF Therapy

Emily K. Wu, MS[1,2], **Zoe I. Henkes, BS**[2], **Brion McGowan, MD**[2], **Richard D. Bell, MS**[2,3], **Moises J. Velez, MD**[3], **Alexandra M. Livingstone, PhD**[1], **Christopher T. Ritchlin, MD, MPH**[4], **Edward M. Schwarz, PhD**[1,2,5], **Homaira Rahimi, MD**[2,6]

[1]Department of Microbiology and Immunology, University of Rochester School of Medicine and Dentistry, Rochester, NY

[2]Center for Musculoskeletal Research, University of Rochester School of Medicine and Dentistry, Rochester, NY

[3]Department of Pathology and Laboratory Medicine, University of Rochester School of Medicine and Dentistry, Rochester, NY

[4]Department of Medicine, Allergy/Immunology and Rheumatology, University of Rochester School of Medicine and Dentistry, Rochester, NY

[5]Department of Orthopaedics, University of Rochester School of Medicine and Dentistry, Rochester, NY

[6]Department of Pediatrics, University of Rochester School of Medicine and Dentistry, Rochester, NY

Abstract

Interstitial lung disease (ILD) is a well-known extra-articular manifestation of rheumatoid arthritis (RA). RA-associated ILD (RA-ILD) exists on a wide spectrum, with variable levels of inflammatory and fibrotic activity, although all subtypes are regarded as irreversible pathology. In both articular and pulmonary manifestations, tumor necrosis factor (TNF) is a significant pathogenic factor. While anti-TNF therapy ameliorates joint pathology, it exacerbates fibrotic RA-ILD. The TNF-transgenic (TNF-Tg) murine model of RA develops both inflammatory arthritis and an ILD which mimics a cellular non-specific interstitial pneumonia (NSIP) pattern dominated by an interstitial accumulation of inflammatory cells with minimal to absent fibrosis. Given the model's potential to elucidate the genesis of inflammatory RA-ILD, we aim to: 1) characterize the cellular accumulations in TNF-Tg lungs, and 2) assess the reversibility of inflammatory ILD

Corresponding Author: Homaira Rahimi, MD, Address: 601 Elmwood Ave, Box 777, Rochester, NY 14642, T: 585 275 4733, F: 585 271 7512, Homaira_Rahimi@URMC.Rochester.edu.

Author Contributions: E.K.W., A.M.L, E.M.S., and H.R. contributed significantly to experimental conception and design; E.K.W., Z.I.H, B.M., R.D.B. contributed to experimental development and data collection; E.K.W., M.J.V., A.M.L. contributed to data analysis; E.K.W., R.D.B, C.T.R, H.R., and E.M.S. contributed to data analysis; and E.K.W. drafted the manuscript.

All parties have no conflicts of interest to disclose.

following anti-TNF therapy known to resolve TNF-Tg inflammatory arthritis. TNF-Tg mice with established disease were randomized to anti-TNF or placebo therapy, and evaluated with imaging, histology, and flow cytometric analyses, together with WT controls. Flow cytometry of TNF-Tg vs. WT lungs revealed significant increases in activated monocytes, conventional dendritic cells (cDC2), and $CD21^{+}/CD23^{-}$ B cells that are phenotypically distinct from the Bin cells which are known to accumulate in joint draining lymph nodes. In contrast to human RA-ILD, anti-TNF treatment significantly ameliorated both joint and lung inflammation. These results identify a potential role for activated monocytes, cDC2, and $CD21^{+}/CD23^{-}$ B cells in the genesis of RA-ILD, which exist in a previously unknown, reversible, pre-fibrotic stage of the disease.

Introduction

Rheumatoid arthritis (RA) is a chronic and systemic inflammatory disease estimated to affect 1% of the world's population (1–4). Outside of the well-known inflammatory articular involvement, RA is often accompanied by a number of systemic manifestations. These include inflammatory nodules, cardiovascular disease, and pulmonary involvement (5). In particular, interstitial lung disease (ILD) is one of the primary extra-articular manifestations in RA. RA-associated ILD (RA-ILD) is a leading cause of morbidity and mortality in RA patients (5–9). This process is progressive and considered to be largely irreversible.

RA-ILD has two predominant subtypes as determined by chest CT imaging and histologic features. These subtypes include the usual interstitial pneumonia (UIP) pattern, which exhibits a predominantly fibrotic disease process, and the non-specific interstitial pneumonia (NSIP) pattern, which is more inflammatory in nature (9–20). The UIP pattern is the predominant subtype identified in RA-ILD cases and is comprised of notable dense fibrosis with remodeling of the lung architecture. NSIP, the second-most prevalent subtype, is defined by the presence of diffuse and symmetric chronic interstitial inflammation, with retained lung architecture and less fibrotic change (21).

The factors that underlie the development and progression of ILD remains enigmatic. A large body of evidence supports the complex role of both genetic and environmental factors in the pathogenesis of RA-ILD, but the etiology remains widely unknown (22–27). One theory of pathogenesis postulates that the pulmonary disease manifests in two sequential stages over time. This progressive pathology involves a primary exacerbation, which initiates an inflammatory state predominated by cellular infiltration, leading to an NSIP pattern of pathology. This is followed by secondary environmental triggers leading to fibrotic change in the peripheral pulmonary tissue, consistent with a UIP pattern (28, 29). The idea of distinct stages of progressive disease fits well with the previously addressed epidemiologic studies looking at the specific subsets of RA-ILD. However, clinical evidence for this model is difficult to attain, since most patients are diagnosed following symptom presentation, when more advanced fibrotic changes are already established and lung function is significantly compromised. Given the limitations related to screening for ILD in RA patients, identifying a cohort of patients with early changes on lung imaging to study disease progression prior to symptom manifestation presents a formidable challenge.

Tumor necrosis factor (TNF) is an appealing target in RA-ILD because it is a pivotal cytokine in the development and perpetuation of both articular (27, 30, 31) and pulmonary inflammation (32–35). Furthermore, elucidating the function of TNF in pulmonary pathology associated with underlying RA is particularly crucial due to the central importance of TNF inhibition in treating joint inflammation. As previously discussed, TNF overexpression is associated with a variety of phenotypes; yet it is known that RA-ILD can progress and even worsen (particularly the fibrotic component) in patients with RA taking anti-TNF agents (36–42). Regrettably, the reports on progressive fibrosis do not comment on alterations of interstitial inflammation in the lung of RA-ILD patients on anti-TNF therapy. It is certainly plausible that anti-TNF therapy during the inflammatory phase of ILD proposed in the previously described model (28) may block the progression to lung fibrosis and challenge the irreversibility of this disorder. Understanding how TNF influences lung inflammation and fibrosis is critical due to anti-TNF therapy's role as a cornerstone of RA treatment.

We work with the TNF-transgenic (TNF-Tg) mouse model (43, 44), which produces systemic TNF over-production that causes inflammatory erosive arthritis and ILD. Data support the concept that TNF mediates some aspects of pulmonary pathology, but the specific aspects induced through TNF signaling are unknown. To address this gap, we: 1) identified the inflammatory cells that accumulate in the lungs of TNF-Tg mice during the genesis of ILD, and 2) examined the "irreversible" nature of inflammatory ILD in this mouse model of RA using anti-TNF therapy on established disease. Our results demonstrate a significant increase in activated monocytes and conventional dendritic cells (cDC2) in the lungs isolated from TNF-Tg mice with inflammatory ILD. We also identified $CD21^{+}/CD23^{-}$ B cells, which are phenotypically distinct from the $CD21^{hi}/CD23^{+}$ B cells in inflamed nodes (Bin cells) that accumulate in joint draining lymph nodes of TNF-Tg mice (45) and RA patients (46). In contrast to human RA-ILD, anti-TNF treatment significantly ameliorates both joint and lung inflammation. Taken together, these results identify a potential role for activated monocytes, cDC2, and $CD21^{+}/CD23^{-}$ B cells in the genesis of RA-ILD, which are restricted to a previously unknown reversible pre-fibrotic stage of the disease.

Methods

Animals

All animal research was conducted using protocols approved by the University of Rochester Institutional Animal Care and Use Committee. The 3647-line tumor necrosis factor transgenic (TNF-Tg) mouse systemically overexpresses a single copy of the human TNF gene. The 3647 TNF-Tg was originally obtained from Dr. George Kollias (Institute of Immunology, Alexander Fleming Biomedical Sciences Research Center, Vari, Greece) (43, 44, 47). Littermate controls were used in all experiments. Mice were screened via micro-computed tomography (μCT) starting at 3 months of age for severe lung disease, as determined by a threshold of >400 mm^3 post-expiratory lung tissue volume. All animals were treated and analyzed using a variety of outcome measures as outlined in Supplemental Figure 1.

Monoclonal Antibody Treatment

All animals were randomized into cohorts (n=6 each) comparing male and female, anti-TNF vs placebo treatment at time of recruitment based on the previously stated threshold of lung disease. All animals were paired at recruitment, with matching initial lung volumes placed in opposite treatment groups. Murine anti-human TNF monoclonal antibody (CNTO12, Centocor R&D, Radnor, PA, USA) or IgG1 isotype placebo control monoclonal antibody (CNTO151, Centocor R&D) were administered at 10mg/kg/wk via I.P. injection for six weeks total, as previously reported (48, 49).

Grip Strength

Grip strength assessment was performed similarly to previous methods (50). Grip strength was assessed at all longitudinal timepoints via a force meter attached to a mesh grate (Chatillon DFE2 Force Gauge, Metek, Largo, FL, USA). Mice were placed on the grate such that their paws could grip the wires while the investigator performed low-force tail pulling to elicit a gripping response. The force generated from the resistance to pull was recorded. The mean value of 5 repeated measures per mouse for each time point was used for statistical analysis. Mouse weight was obtained and recorded together with grip strength.

Ultrasound

3D ultrasound imaging of the popliteal lymph nodes (PLN) was performed using the VisualSonics Vevo3100 (FUIJIFILM, Toronto, ON, Canada). Each mouse was followed longitudinally, with imaging every 2 weeks beginning at week 0 of treatment. B mode images were collected for each animal at each time point. Stacked B mode images were imported into Amira software (ThermoFisher Scientific, Hillsboro, OR, USA), allowing for identification and segmentation of the lymph node from the surrounding tissue. All lymph node volumes were collected and calculated as previously described (51–54).

Micro-Computed Tomography (μCT)

Cross-sectional μCT imaging was performed on all mice prior to initiation of treatment and at completion of treatment (at weeks 0 and 6). μCT of the lungs was performed with the VivaCT 40 (Scanco Medical, Bruttisellen, Switzerland) as previously described (55). Briefly, mice were anesthetized using 1.5–2% Isoflurane (VetOne, Fluriso, Boise, ID, USA) and placed in the prone position in the imaging tube. A blood-pressure transducer (BPS-BTA and SDAQ, Vernier, Beaverton OR) was placed underneath the chest cavity to monitor the chest wall movements as a surrogate measure of the respiratory cycle. A custom, previously cited, non-predictive gating method developed in LabVIEW (National Instruments, Austin, TX, USA) was applied to selectively obtain images during the post-expiratory phase of the breathing cycle to minimize motion artifacts (55). The μCT imaging parameters were: 1000 projections over 180°, 300 milliseconds integration time, 45 kVp, and 176 microamp current. DICOMs at 35 μm^3 isotropic voxel resolution were exported to Amira for image analysis using semi-automated segmentation. All 3-dimensional reconstructions and volume quantifications were performed in Amira software (55, 56).

Histology

At termination, the left lobe of the lung was inflated with 10% neutral buffered formalin (NBF) using a 23G needle and 5mL syringe through the trachea. The left lobe was subsequently incubated in 10% NBF for 3 days before histology processing. The lungs were processed and embedded in paraffin blocks by the University of Rochester Medical Center-Center for Musculoskeletal Research Histology Core Facility. Lungs underwent coronal sectioning from paraffin in 3 consecutive regions, each no less than 100μm apart. Each region was ~100μm thick, each sectioned into a series of 5μm slices. One representative slide from each region was stained with hematoxylin and eosin (H&E). All slides were scanned with an Olympus VS120 (Olympus, Tokyo, Japan). A board-certified pathologist (MV) was blinded and graded each slide on a scale of 0–3 (none, mild, moderate, severe) for perivascular inflammation, interstitial inflammatory infiltrates, alveolar macrophages, and vascular luminal thickness. A total histology score for each slide was generated using the sum of the scores from each sub-category for a total scale range of 0–12. Values from each individual subject were averaged together for data analysis.

Knees collected at termination were fixed in 10% NBF for three days prior to histologic processing and paraffin embedding. Samples were sectioned on a sagittal plane in three distinct regions 50 μm apart. Each region had five 5 μm-thick sections. Representative slides from each region were similarly stained with H&E and scanned with an Olympus VS120. Quantification of synovial area was performed manually on VisioPharm software (VisioPharm, Hoersholm, Demark).

B220 immunohistochemical staining was performed on all lungs using PE-conjugated B220 antibody (Biolegend, San Diego, CA, USA) and NucBlue Live Cell nuclear staining (Invitrogen, Eugene, OR, USA). Semiautomated histomorphometry was performed to manually identify and gate $B220^+$ follicle-like structures within the total lung area of each stained slide. Histomorphometric analysis was used to quantify both total number of follicles per lung and follicle area. All B220-staining histomorphometric analysis was performed using QuPath software (Queen's University, Belfast, Ireland).

Flow Cytometric Analysis

Lungs were extracted for the use of both flow cytometric analysis and histologic evaluation. Prior to inflation for histologic analysis, the right lobes were tied off using surgical sutures and peripheral lung tissue removed for processing into a single-cell suspension. The right lobes were taken and manually digested using a razor blade before being incubated with 1 mL of 0.2 mg/mL Liberase (Sigma, St. Louis, MO, USA) with 0.75 KU/mL DNAse IV (Sigma) in RPMI buffer at 37°C for 30 minutes. Homogenized lungs were passed through a 70 μm nylon mesh filter to create a single-cell suspension and washed in 2% FBS 2.5uM EDTA in PBS. ACK lysis buffer (recipe from Cold Spring Harbor) was used to lyse the remaining RBCs in the suspension. Cells were counted on a hemocytometer (Hausser Scientific, Horsham, PA, USA) using trypan blue in a 1:1 dilution.

Cells were blocked with 2 μg/mL Fc block (BioXcell, West Lebanon, NH, USA) for 10 min prior to labelling. 1 mg/mL Live/Dead-Aqua (Invitrogen) was used as a viability stain. Cells

were subsequently labelled with a set of fluorochrome-conjugated antibodies for cell surface markers at various optimized concentrations based on previously published panels (57, 58). These included CD3-APC-Cy7 (clone: 17A2, Biolegend, San Diego, CA, USA), CD19-APC (clone: 1D3/CD19, Biolegend), CD11b-PE (clone: M1/70, BD Biosciences, San Jose, CA USA), CD11c-eF450 (clone: F418, eBioscience, San Diego, CA, USA), CD45-BV786 (clone 30-F11, BD Biosciences), MHCII-FITC (clone M5/114.15.2, eBioscience), Siglec F-PE-CD594 (clone E50–2440, BD Biosciences), anti-F4/80-FITC (clone BM8, BioLegend), anti-CD88 APC (clone 20/70, BioLegend), anti-CD64 BV605 (clone X54–5/7.1, BioLegend), anti-XCR1 BV650 (clone ZET, BioLegend), and anti-CD172a PE-Dazzle-594 (clone P84, BioLegend),. A second panel examining the B cell populations followed the same protocol, using CD1d-APC (clone: 1B1, Biolegend), CD3-APC-Cy7 (clone: 17A2, Biolegend), CD19-PE-Cy5 (clone: 6D5, Biolegend), CD45R/B220-BV785 (clone: RA3–6B2, Biolegend), CD21/CD35-PE (clone: 7E9, Biolegend). CD23-FITC (clone: B3B4, Biolegend).

Data acquisition was performed on a BD LSR II 18-color flow cytometer using BD FACSDiva software (BD Biosciences). Data analysis and compensation calculations were performed using FlowJo software (TreeStar, Ashland, OR, USA). Cell populations were evaluated based on a sequential gating strategy (see Fig. 1). The data was analyzed and presented as a percentage of live cells based on Live/Dead staining.

Statistics

All statistics were performed in Prism 7.00 (GraphPad Software, La Jolla, CA, USA). Unless otherwise stated, all continuous variables were analyzed using a 2-way ANOVA with Tukey's post hoc on multiple comparisons to examine the effects of both sex (female vs male) and treatment (placebo vs anti-TNF).

Results

Identification of myeloid population shifts present in TNF-Tg mice

Flow cytometric analysis was performed on the pulmonary tissue of both TNF-Tg mice and their WT littermates to identify the cellular populations responsible for the lung pathology. Sequential gating (Fig. 1A–G) was performed to find differences in specific cell populations. The identified populations were labeled as outlined in Fig. 1H. These populations include alveolar macrophages, two subsets of conventional dendritic cells (cDC1s and cDC2s), and monocytes at various stages of activation. For proportionate changes in the total cellular composition, representative contour plots for WT and TNF-Tg mice of the CD11b vs CD11c profile demonstrated gross differences in the myeloid populations in disease (Fig. 1I and 1J). More specifically, large increases were found in the $CD11b^{++}$ $CD11c^{++}$ (Population 2) and $CD11b^{++}$ $CD11c^{+}$ (Population 3) cells (Fig. 1I and 1J). Positive staining with the cell surface markers MHCII and Siglec F found these cells as consistent with cDC2 cells and activated monocytes/macrophages (Populations 2 and 3, respectively) (Fig. 1H). Additional characterization markers for DC subsets and macrophages confirmed these findings (Supplemental Fig. 2 and 3).

Anti-TNF therapy ameliorates systemic effects

Previous studies have monitored the effects of anti-TNF therapy on the systemic and articular pathologies in the TNF-Tg model (48, 49, 59, 60). For the 3647 line specifically, it was found that the maximum efficacy of treatment was attained at 6 weeks of therapy (48, 49). To confirm the effectiveness of anti-TNF therapy on systemic effects, total body weight was monitored at each week of the treatment course, beginning at Week 0, just prior to initiation of treatment. Baseline weight at beginning of treatment was identical within sex between the cohorts (Fig. 2A). Total body weight continuously declined over time in the placebo-treated TNF-Tg females, consistent with disease progression. In contrast, the male TNF-Tg placebo-treated cohort maintained a consistent body weight consistent with previous reports (50), while both anti-TNF treated cohorts continuously gained weight over the 6-week course (Week 0 vs Week 6, Males, $p=0.0025$; Females, $p<0.0001$, Fig. 2A).

Grip strength was monitored over time on a bi-weekly basis to monitor gross arthritic change in the smaller peripheral joints. Grip strength was identical within each sex between treatment groups at baseline, but significantly increased in the anti-TNF treated animals compared to placebo for both male and female cohorts over time (Fig. 2B). Mice treated with anti-TNF therapy demonstrated improved grip strength compared to baseline at points as early as 2 weeks into treatment (Fig. 2B).

Histomorphometry performed on H&E sections of the knee joint revealed that total synovial area, a measure of active synovitis, was significantly reduced in anti-TNF treated mice as compared to their placebo control counterparts ($p<0.0001$ for both sexes) (Fig. 2C–G).

Assessment of total volume of the popliteal lymph nodes is another non-invasive marker of arthritic activity in the TNF-Tg model (54, 60, 61). During the development of active inflammation in these mice, the draining lymph node of the affected joint expands in size due to the increase in lymphatic trafficking from the synovial space. We utilized ultrasound imaging and virtual 3D reconstruction to quantify the total volume of the lymph node as a marker of disease progression and activity in the context of both animal models and clinical patients (54, 61, 62). Representative 3D reconstructions of popliteal lymph nodes (PLNs) shown in Fig. 2H–K demonstrate a marked difference between placebo and anti-TNF mice by the end of treatment. Similar to the grip strength results, longitudinal quantification of the total PLN volumes demonstrated a marked initial decrease in PLN volume in the anti-TNF cohorts, with a significant difference in volume between treatment groups maintained over the course of treatment for both sexes (Fig. 2L). The improved arthritis assessments indicate the amelioration of symptoms and confirm efficacy of treatment with anti-TNF therapy in this model.

Anti-TNF therapy restores lung volume and is associated with clearance of cellular infiltrates

3D micro-computed tomography (μCT) is a validated *in vivo* method for measuring total tissue volume of the lung (55). Increased lung tissue volumes were observed in TNF-Tg mice compared to WT littermates (55). To document the presence and severity of lung disease and the effects of anti-TNF therapy on pulmonary inflammation, μCT imaging was

performed prior to treatment initiation and prior to termination. Representative 3D reconstructions of female placebo-treated (Fig. 3A and 3C) and anti-TNF-treated lungs (Fig. 3B and 3D) at Week 0 (Fig. 3A and 3B) and Week 6 (Fig. 3C and 3D) revealed that anti-TNF treated lungs demonstrated a markedly decreased tissue mass. Quantification of the lung tissue volume via thresholding on μCT Hounsfield units shows significant reduction in lung tissue volume and improvement in the anti-TNF treated cohorts of both sexes at the end of treatment (Fig. 2E, anti-TNF Week 0 vs Week 6, female, 469.0 ± 28.6 vs 292.0 ± 31.7 mm^3, male, 437.5 ± 33.1 vs 292.2 ± 38.8 mm^3, M ± SD, $p<0.0001$).

It should be noted that μCT imaging is limited by resolution thresholds. “Tissue volume” changes for these scans could therefore be attributed to alterations in fluid accumulation, cellular mass, or collagen deposition. To qualitatively interrogate the change in composition, histology was performed on the lung tissue (Fig. 4A–G). H&E staining revealed an inflammatory pathology, with no signs of fibrotic change in the parenchymal tissue (data not shown). Four characteristic pathologic patterns were identified in the lung, including interstitial inflammatory infiltrate, vascular luminal thickening, perivascular inflammation, and the formation of follicle-like structures lacking a germinal center (representative examples in Fig. 4A), all consistent with previous reports (50, 63).

To demonstrate the level of inflammation and cellular accumulation present at 3 months of age (Fig. 4B and 4E) we obtained representative H&E sections of both female and male age-matched TNF-Tg animals from a different experimental cohort. Following the 6-week treatment course, histological analysis of placebo-treated and anti-TNF treated lungs from both females and males confirmed the findings on μCT. Anti-TNF treated lungs showed marked decreases in both the total cellular infiltrate and the previously noted pathologic patterns as compared to their placebo-treated counterparts (Fig. 4C vs 4D; 4F vs 4G). Clinical grading of representative slides from each animal for individual pathologic features confirmed the effects of anti-TNF therapy, with significant decreases in total histology scores for both female and male mice (Fig. 4H, placebo vs anti-TNF, females, 7.88 ± 1.88 vs 3.33 ± 1.20; males, 5.72 ± 1.24 vs 2.89 ± 1.29, M ± SD, ****$p<0.0001$). Notably, while total scores differed between females and males with placebo treatment ($p<0.0001$), no significant difference was noted between the sexes with anti-TNF treatment ($p=0.7361$). Sub-scoring for individual histologic patterns exposed to anti-TNF treatment showed a significant decline in interstitial inflammatory infiltrates (Fig. 4I) and alveolar macrophages (Fig. 4J). Vascular patterns were less drastically affected by treatment. Perivascular inflammation (Fig. 4K) in male cohorts and vascular luminal thickness in the female cohorts (Fig. 4L) each decreased significantly.

The interstitial inflammatory infiltrate, the perivascular inflammatory infiltrate, and the vascular luminal thickening appeared to be almost completely ameliorated with treatment. The follicle-like structures alone remain in the treated lungs. However, these structures are attenuated, with decreased absolute numbers of these structures appearing in the anti-TNF treated lungs (Fig. 5H). Importantly, for both calculated tissue volume measured by μCT and histologic evaluation, anti-TNF therapy ceases progression of the disease and treats the baseline pathology.

B cell populations of the TNF-Tg lung are not cleared with anti-TNF therapy

Previous studies of the arthritic joint-draining lymph node from the lab implicated a specific B cell subset, Bin cells (B cells in inflamed nodes), as a key effector cell that promotes both structural and inflammatory changes in the draining lymph nodes of inflamed joints (45, 64). This unique population is a sub-population of B cells defined by their CD21/35^{hi}CD23^{+} expression profile, and were targeted to the sites of active articular disease activity. They are associated with the onset of inflammatory-erosive arthritis, and reflect arthritic activity in the affected joint. Subsequent B cell depletion was unexpectedly found to ameliorate symptoms, suggesting that they play an active role in disease pathogenesis (45, 64).

The majority, but not all, of the pathologic patterns noted in terminal disease were obliterated with anti-TNF therapy. Of the four noted patterns, only the follicle-like structures remained after treatment administration. Analogous to the lymphatic system, we wondered if these follicles contained cellular compositions similar to the latent populations found in the draining lymph nodes. B220 (CD45R) IHC staining uncovered the presence of B cells in the follicle-like structures in the pulmonary tissue prior to treatment initiation (3-month-old representative samples) and in both the placebo and anti-TNF treated cohorts (Fig. 5A–C). Histomorphometry analysis was performed on the lungs using semiautomated gating to identify and quantify B220^{+} follicle number and area for each lung (Fig. 5D and 5E). For anti-TNF treated mice, total follicle area (as a percentage of total lung area), average follicle area, and the number of follicles per lung were decreased compared to placebo-treated counterparts (Fig. 5F–H).

Further investigations regarding the existence and possible role of the Bin population in pulmonary manifestations in the TNF-Tg model were performed. Flow cytometric analysis interrogating the phenotype of these B cell accumulations was performed (45, 65), defining follicular B cells (CD21/35^{low}CD23^{+}), marginal zone B cells (CD21/35^{hi}CD23^{low}), and Bin cells (CD21^{+} CD23^{hi}). Flow cytometry revealed a different B cell profile in the diseased untreated TNF-Tg lung than the one observed in the peripheral lymph node (Fig. 5I–L). Most notably, the pulmonary B cells displayed a decreased expression of CD23 (Fig. 5L). Therefore, these structures remain in the lung despite therapeutic intervention as hypothesized, but the profile of these B cell populations differs from that which is present on B lymphocytes found in the lymphatic system.

Selectively increased populations of Monocytes and Dendritic Cells in the TNF-Tg lung return to WT levels with anti-TNF therapy

Total cell count for the lungs was significantly increased in the placebo treated cohort when compared to both WT controls and anti-TNF treated mice (Fig. 6G). It should be noted that the cell counts in the anti-TNF treated cohorts declined to the level of WT animals, with no significant difference found between these groups for either female or male mice.

To further assess the proportionate shifts in the pulmonary cell populations with treatment, flow cytometric analysis was performed using the earlier panel and gating scheme (Fig. 1A–H) that identified populations of interest. Representative contour plots of the myeloid profile (again using CD11b vs CD11c) comparing age-matched WT littermate, placebo treated, and

anti-TNF treated lungs demonstrate differences in the populations of each cohort (Fig. 6A–F). Consistent with our earlier analysis, the placebo treated TNF-Tg mice demonstrated disproportionate increases in the $CD11b^{++}$ $CD11c^{++}$ $MHCII^{+}$ Siglec F^{-} (Population 2, cDC2) and $CD11b^{++}$ $CD11c^{+}$ $MHCII^{int}$ Siglec F^{-} (Population 3, activated monocyte/macrophage) cells. In comparison, the anti-TNF treated mice had cellular profiles similar to the WT littermate counterparts.

Analysis of the populations as percentages of Live $CD45^{+}$ cells (Fig. 6H–O) and absolute numbers of cell subsets (Supplemental Table 1) confirm that the most significant changes are within the cDC2 and activated monocyte/macrophage populations (Fig. 6L and 6M). These findings support our initial impressions, confirming that these two populations disproportionately changed in the TNF-Tg lung, and returned to WT levels with anti-TNF therapy.

Discussion

In this study, we find that: 1) anti-TNF therapy both prevented progression and ameliorated pre-existing pathology in pulmonary tissue, and 2) treatment of pathology involved the shifting of the cellular composition of the diseased lung to WT-like levels.

Six weeks of anti-TNF therapy decreased lung tissue volume with resolution of inflammatory cellular infiltration in TNF-Tg mice of both sexes, which was not observed in placebo treated animals. The treatment lessened interstitial cellular accumulation, and the cell populations returned to WT levels. We identified two distinct myeloid populations in the lung which were disproportionately up-regulated in disease and remain elevated following anti-TNF therapy. Flow cytometric analysis of the lung found that these two populations were consistently elevated in the pathologic state, and were identified as activated monocytes/macrophages and cDC2 cells. B cell-based follicle-like structures were noted to be ameliorated in both absolute number and size, yet remained despite anti-TNF treatment. These B cells were found to be distinct from the Bin population, a population which was previously implicated in promoting and facilitating active articular disease in this mouse model. Future studies aimed to further evaluate the role of these immune cell populations will include depletion of the key immune cells. Taken together, these results suggest that the inflammatory stage of ILD is mediated by a limited number of key populations, and that the cellular component of RA-ILD is responsive to anti-TNF therapy.

RA-ILD is generally considered an irreversible pathology, with variable amounts of fibrotic change, which is the component that is resistant to treatment. The previously discussed theory of RA-ILD's progression through distinct stages of disease suggests that a prior inflammatory state may be necessary for further disease development, and could be reversible with anti-inflammatory therapies.

That being said, it has previously been reported that anti-TNF therapy is ineffective, and possibly detrimental, in the context of RA-ILD (36–42). In the literature, the relationship between anti-TNF therapy and RA-ILD is complex and conflicting. Several articles report differences in ILD diagnosis or outcome with treatment (36, 38–41); however, others have

found no associated risk with anti-TNF therapy (66–68). These studies clarify that pre-existing pulmonary impairment was strongly associated with the increased risk of adverse reactions and anti-TNF treatment often exacerbated a previously diagnosed lung disease, although the inflammatory or fibrotic nature of the pathology was not specified. When anti-TNF therapy accelerates disease progression, it is specifically in the context of fibrotic change in the lung (41, 69). One possible explanation for this phenomenon is TNF's ability to inhibit TGF-β signaling (70–72), coupled with TGF-β's role in promoting fibrotic disease (73). These findings led to the current guidelines stipulating the cessation of all anti-TNF therapies in RA patients diagnosed with ILD. This restriction severely limits the available treatment for the articular symptoms of RA.

One of the most notable results from this study was the reversal of pre-existing inflammation on top of the prevention of disease progression with the anti-TNF regimen. Given the two-stage hypothesis of RA-ILD development, the reversal of inflammatory pulmonary pathology in the TNF-Tg mouse in this study could have broader implications on the current clinical guidelines regarding the risk of anti-TNF therapy in RA-ILD. The TNF-Tg model isolates an important inflammatory component of the RA-ILD phenotype. In the context of the theory of RA-ILD progression, our results regarding the reversal of inflammatory components of ILD implies a more nuanced interpretation of clinical data. While anti-TNF therapy may be contraindicated for irreversible fibrotic changes in the lung, implementation of anti-TNF therapies at an earlier, purely inflammatory stage of disease may lead to complete amelioration of pulmonary pathology. Of course, this would require identifying patients with ILD prior to fibrosis onset, which has been difficult to date, and current screening guidelines have not sufficiently captured this population.

A second-line biological therapy for the articular disease in RA is rituximab, a chimeric anti-CD20 antibody that targets B lymphocytes for the treatment of RA (74). RA-ILD bronchoalveolar lavage fluid showed plasma cells and this finding combined with the efficacy of B cell depletion for arthritis catalyzed several studies that evaluated rituximab to treat RA-ILD (75–77). Overall, positive responses to anti-B cell therapy were observed for both UIP and NSIP subtypes, although responses in patients with severe UIP was not as robust (76). The reasons for the responsiveness to anti-B cell therapy remains unclear. Our current findings suggest that the presence of these B cell accumulations in the lung tissue, may reflect inducible bronchus associated lymphoid tissue also found in other TNF over-expressing mouse models (78). These tissues may be playing a role in either onset of the inflammatory processes in the lung or persistence of the disease state. However, further studies are necessary to fully elucidate the role of B cell accumulations in this mouse model.

Several limitations of this study are noted. First, while we have identified two target cell populations of interest from our myeloid panel, these characterizations are limited. Our flow panel was based on prior publications characterizing the cellular composition of pulmonary tissue to create a general profile of our TNF-Tg lungs. The original intention of the panels was to create a general, broad profile of the composition of the lung, which was also our goal for this study. However, to delve more deeply into the specific roles these cells play in mediating the pathogenesis of our model, more specific characterization is required. Future directions regarding the roles of these populations would ideally include longitudinal studies

looking at the progression of disease over time, as well as methods of accumulation (such as peripheral migration, proliferation of local populations, etc).

The second issue regards the isolated nature of our model. The TNF-Tg mouse model expresses human TNF in a dysregulated manner, leading to the subsequent systemic inflammatory effects mimicking inflammatory arthritis. Anti-TNF therapy should therefore ameliorate any acute inflammation, as shown in prior studies looking at joint inflammation in these mice. (49, 59, 60). Given the pervasive nature of TNF in RA, it would follow that TNF would play an integral role in the predisposition towards pulmonary involvement as part of the systemic manifestations of disease. In fact, recent clinical data from Sparks et al. found an association between RA disease activity and increased risk of RA-ILD development (79). However, the pulmonary pathology of the TNF-Tg model has not been expansively characterized in the context of the systemic extra-articular inflammation. Our lab has previously described the inflammatory nature of this model, with little to no fibrotic involvement of the pulmonary interstitium (50, 55). Our model provides a focused perspective on an isolated component of RA-ILD's complex manifestation. Indeed, our results showed both cessation of disease progression as well as reversal of pre-existing infiltration in the pulmonary tissue (Fig. 2 and 3).

This brings us to an interesting point with regards to our model and its possible implications regarding the development of fibrotic disease. Multiple publications have described the induction of pulmonary fibrosis in the surfactant protein-C/TNF transgenic (Sp-C/TNF) murine model, a similar yet more localized form of the TNF-Tg model in which TNF-α expression is controlled by the surfactant protein-C promoter, resulting in TNF overexpression in the pulmonary tissue (70, 78, 80–82). The Sp-C/TNF-Tg model is documented as having a lymphocytic infiltrate, which progresses to a variable fibrosing alveolitis with significant inflammation, diffuse interstitial collagen deposition, and emphysematous changes. This finding stands in stark contrast to our systemic TNF- Tg model, which exhibits a solely inflammatory phenotype with diffuse cellular accumulation in the interstitium (55, 63). Furthermore, a third model with inducible TNF expression in the lung develops emphysematous change with lymphoid follicles and no signs of augmented collagen deposition in the pulmonary tissue (78). Each model outlined above demonstrates significant and varied pathologic change on the pulmonary physiology, complicating our understanding of TNF's effects in lung disease. The discordance of the phenotypes between the models raises important questions regarding the contribution of TNF in human RA-ILD, and could provide clues to the transition between inflammatory and fibrotic disease.

One important point to note is that fibrosis is inherently a chronic and prolonged process, taking months to years to develop in clinical RA-ILD. Systemic TNF-Tg females have previously been found to have lifespans of 5.5 months. Compounded with the constitutive inhibition of TGF-β signaling by TNF (70–72), these factors provide the most likely explanation for the lack of fibrosis in the TNF-Tg model. Further studies regarding the role of TNF in RA-ILD development may benefit from a direct comparison of all the models' local cytokine expression profiles. This approach could provide evidence towards the etiology of the different terminal disease phenotypes.

In conclusion, we have shown that anti-TNF therapy ameliorates pre-existing inflammatory pulmonary pathology and identified two distinctly up-regulated myeloid populations of interest in the pulmonary cellular accumulation. Evaluation via μCT and histology both confirmed that anti-TNF therapy effectively reversed pre-existing inflammation in the lung, reducing cellular infiltration back to WT levels. Concurrent flow cytometric analysis confirmed the post-treatment lung composition as comparable to WT cellular profiles, indicating the removal of selective pathogenic cells. These included the disproportionately up-regulated monocytes/macrophages and the cDC2-like populations, along with focal B cell accumulations in the lung parenchyma, which were all attenuated with anti-TNF treatment. Further studies demand the rigorous characterization of our populations of interest, and further exploration of more nuanced clinical guidelines regarding anti-TNF therapies in the treatment of RA-ILD.

Supplementary Material

Refer to Web version on PubMed Central for supplementary material.

Acknowledgments

The authors would like to thank Mike Thullen in the Biomechanics, Biomaterials, and Multimodal Tissue Imaging (BBMTI) Core at the University of Rochester Medical Center for his technical expertise performing the μCT scans. The authors would also like to acknowledge Kathy Maltby and Jeff Fox in the Histology, Biochemistry and Molecular Imaging (HBMI) Core at the University of Rochester Medical Center for their technical expertise with the histology performed herein. The anti-TNF and placebo monoclonal antibodies used in this study were provided by Janssen Pharmaceuticals Inc.

Grants and Other Financial Support: NIH/NIAMS T32 AR053459, NIH/NIAMS P30 AR069655, NIH/NIAMS K08 AR067885, NIH/NIAMS R01 AR56702, NIH/NICHD HD068373, NIH/NIA R01 AG051456, NIH/NCI R01 CA220467

This work was funded by grants from NIH MSTP T32 GM007356, NIH/NIAMS T32 AR053459, NIH/NIAMS P30 AR069655, NIH/NIAMS K08 AR067885, and NIH/NIAMS R01 AR56702.

Abbreviations List

cDC	Conventional Dendritic Cell
H&E	Hemotoxylin & Eosin
ILD	Interstitial Lung Disease
NBF	Neutral Buffered Formalin
NSIP	Non-specific Interstitial Pneumonia
PLN	Popliteal Lymph Node
RA	Rheumatoid Arthritis
RA-ILD	Rheumatoid Arthritis-associated Interstitial Lung Disease
Sp-C/TNF	Surfactant protein-C/TNF Transgenic mouse model
TGF-β	Tumor Growth Factor- Beta

TNF	Tumor Necrosis Factor
TNF-Tg	Tumor Necrosis Factor Transgenic mouse model
μCT	Micro-Computed Tomography
UIP	Usual Interstitial Pneumonia

References

1. Gibofsky A 2012 Overview of epidemiology, pathophysiology, and diagnosis of rheumatoid arthritis. Am J Manag Care 18: S295–302. [PubMed: 23327517]
2. Helmick CG, Felson DT, Lawrence RC, Gabriel S, Hirsch R, Kwoh CK, Liang MH, Kremers HM, Mayes MD, Merkel PA, Pillemer SR, Reveille JD, Stone JH, and W. National Arthritis Data. 2008 Estimates of the prevalence of arthritis and other rheumatic conditions in the United States. Part I. Arthritis Rheum 58: 15–25. [PubMed: 18163481]
3. Hochberg MC, and Spector TD. 1990 Epidemiology of rheumatoid arthritis: update. Epidemiol Rev 12: 247–252. [PubMed: 2286222]
4. Gibofsky A 2014 Epidemiology, pathophysiology, and diagnosis of rheumatoid arthritis: A Synopsis. Am J Manag Care 20: S128–135. [PubMed: 25180621]
5. Sparks JA, Chang SC, Liao KP, Lu B, Fine AR, Solomon DH, Costenbader KH, and Karlson EW. 2016 Rheumatoid Arthritis and Mortality Among Women During 36 Years of Prospective Follow-Up: Results From the Nurses' Health Study. Arthritis Care Res (Hoboken) 68: 753–762. [PubMed: 26473946]
6. Olson AL, Swigris JJ, Sprunger DB, Fischer A, Fernandez-Perez ER, Solomon J, Murphy J, Cohen M, Raghu G, and Brown KK. 2011 Rheumatoid arthritis-interstitial lung disease-associated mortality. Am J Respir Crit Care Med 183: 372–378. [PubMed: 20851924]
7. Assayag D, Lubin M, Lee JS, King TE, Collard HR, and Ryerson CJ. 2014 Predictors of mortality in rheumatoid arthritis-related interstitial lung disease. Respirology 19: 493–500. [PubMed: 24372981]
8. Gabriel SE, Crowson CS, Kremers HM, Doran MF, Turesson C, O'Fallon WM, and Matteson EL. 2003 Survival in rheumatoid arthritis: a population-based analysis of trends over 40 years. Arthritis Rheum 48: 54–58. [PubMed: 12528103]
9. Bongartz T, Nannini C, Medina-Velasquez YF, Achenbach SJ, Crowson CS, Ryu JH, Vassallo R, Gabriel SE, and Matteson EL. 2010 Incidence and mortality of interstitial lung disease in rheumatoid arthritis: a population-based study. Arthritis Rheum 62: 1583–1591. [PubMed: 20155830]
10. Lee HK, Kim DS, Yoo B, Seo JB, Rho JY, Colby TV, and Kitaichi M. 2005 Histopathologic pattern and clinical features of rheumatoid arthritis-associated interstitial lung disease. Chest 127: 2019–2027. [PubMed: 15947315]
11. Doyle TJ, and Dellaripa PF. 2017 Lung Manifestations in the Rheumatic Diseases. Chest.
12. Solomon JJ, Chung JH, Cosgrove GP, Demoruelle MK, Fernandez-Perez ER, Fischer A, Frankel SK, Hobbs SB, Huie TJ, Ketzer J, Mannina A, Olson AL, Russell G, Tsuchiya Y, Yunt ZX, Zelarney PT, Brown KK, and Swigris JJ. 2016 Predictors of mortality in rheumatoid arthritis-associated interstitial lung disease. Eur Respir J 47: 588–596. [PubMed: 26585429]
13. Solomon JJ, Ryu JH, Tazelaar HD, Myers JL, Tuder R, Cool CD, Curran-Everett D, Fischer A, Swigris JJ, and Brown KK. 2013 Fibrosing interstitial pneumonia predicts survival in patients with rheumatoid arthritis-associated interstitial lung disease (RA-ILD). Respir Med 107: 1247–1252. [PubMed: 23791462]
14. Zamora-Legoff JA, Krause ML, Crowson CS, Ryu JH, and Matteson EL. 2017 Patterns of interstitial lung disease and mortality in rheumatoid arthritis. Rheumatology (Oxford) 56: 344–350. [PubMed: 27940586]

15. Nurmi HM, Purokivi MK, Karkkainen MS, Kettunen HP, Selander TA, and Kaarteenaho RL. 2016 Variable course of disease of rheumatoid arthritis-associated usual interstitial pneumonia compared to other subtypes. BMC Pulm Med 16: 107. [PubMed: 27461264]

16. Kelly CA, Saravanan V, Nisar M, Arthanari S, Woodhead FA, Price-Forbes AN, Dawson J, Sathi N, Ahmad Y, Koduri G, Young A, and British N Rheumatoid Interstitial Lung. 2014 Rheumatoid arthritis-related interstitial lung disease: associations, prognostic factors and physiological and radiological characteristics--a large multicentre UK study. Rheumatology (Oxford) 53: 1676–1682. [PubMed: 24758887]

17. Assayag D, Elicker BM, Urbania TH, Colby TV, Kang BH, Ryu JH, King TE, Collard HR, Kim DS, and Lee JS. 2014 Rheumatoid arthritis-associated interstitial lung disease: radiologic identification of usual interstitial pneumonia pattern. Radiology 270: 583–588. [PubMed: 24126367]

18. Yoshinouchi T, Ohtsuki Y, Fujita J, Yamadori I, Bandoh S, Ishida T, and Ueda R. 2005 Nonspecific interstitial pneumonia pattern as pulmonary involvement of rheumatoid arthritis. Rheumatol Int 26: 121–125. [PubMed: 15580351]

19. O'Dwyer DN, Armstrong ME, Cooke G, Dodd JD, Veale DJ, and Donnelly SC. 2013 Rheumatoid Arthritis (RA) associated interstitial lung disease (ILD). Eur J Intern Med 24: 597–603. [PubMed: 23916467]

20. Luukkainen R, Saltyshev M, Pakkasela R, Nordqvist E, Huhtala H, and Hakala M. 1995 Relationship of rheumatoid factor to lung diffusion capacity in smoking and non-smoking patients with rheumatoid arthritis. Scand J Rheumatol 24: 119–120. [PubMed: 7747143]

21. Travis WD, Costabel U, Hansell DM, King TE Jr., Lynch DA, Nicholson AG, Ryerson CJ, Ryu JH, Selman M, Wells AU, Behr J, Bouros D, Brown KK, Colby TV, Collard HR, Cordeiro CR, Cottin V, Crestani B, Drent M, Dudden RF, Egan J, Flaherty K, Hogaboam C, Inoue Y, Johkoh T, Kim DS, Kitaichi M, Loyd J, Martinez FJ, Myers J, Protzko S, Raghu G, Richeldi L, Sverzellati N, Swigris J, Valeyre D, and Pneumonias A. E. C. o. I. I.. 2013 An official American Thoracic Society/European Respiratory Society statement: Update of the international multidisciplinary classification of the idiopathic interstitial pneumonias. Am J Respir Crit Care Med 188: 733–748. [PubMed: 24032382]

22. Klareskog L, Padyukov L, Lorentzen J, and Alfredsson L. 2006 Mechanisms of disease: Genetic susceptibility and environmental triggers in the development of rheumatoid arthritis. Nat Clin Pract Rheumatol 2: 425–433. [PubMed: 16932734]

23. Klareskog L, Padyukov L, Ronnelid J, and Alfredsson L. 2006 Genes, environment and immunity in the development of rheumatoid arthritis. Curr Opin Immunol 18: 650–655. [PubMed: 17010589]

24. Klareskog L, Stolt P, Lundberg K, Kallberg H, Bengtsson C, Grunewald J, Ronnelid J, Harris HE, Ulfgren AK, Rantapaa-Dahlqvist S, Eklund A, Padyukov L, and Alfredsson L. 2006 A new model for an etiology of rheumatoid arthritis: smoking may trigger HLA-DR (shared epitope)-restricted immune reactions to autoantigens modified by citrullination. Arthritis Rheum 54: 38–46. [PubMed: 16385494]

25. Juge PA, Lee JS, Ebstein E, Furukawa H, Dobrinskikh E, Gazal S, Kannengiesser C, Ottaviani S, Oka S, Tohma S, Tsuchiya N, Rojas-Serrano J, Gonzalez-Perez MI, Mejia M, Buendia-Roldan I, Falfan-Valencia R, Ambrocio-Ortiz E, Manali E, Papiris SA, Karageorgas T, Boumpas D, Antoniou K, van Moorsel CHM, van der Vis J, de Man YA, Grutters JC, Wang Y, Borie R, Wemeau-Stervinou L, Wallaert B, Flipo RM, Nunes H, Valeyre D, Saidenberg-Kermanac'h N, Boissier MC, Marchand-Adam S, Frazier A, Richette P, Allanore Y, Sibilia J, Dromer C, Richez C, Schaeverbeke T, Liote H, Thabut G, Nathan N, Amselem S, Soubrier M, Cottin V, Clement A, Deane K, Walts AD, Fingerlin T, Fischer A, Ryu JH, Matteson EL, Niewold TB, Assayag D, Gross A, Wolters P, Schwarz MI, Holers M, Solomon JJ, Doyle T, Rosas IO, Blauwendraat C, Nalls MA, Debray MP, Boileau C, Crestani B, Schwartz DA, and Dieude P. 2018 MUC5B Promoter Variant and Rheumatoid Arthritis with Interstitial Lung Disease. N Engl J Med.

26. Johnson C 2017 Recent advances in the pathogenesis, prediction, and management of rheumatoid arthritis-associated interstitial lung disease. Curr Opin Rheumatol 29: 254–259. [PubMed: 28207496]

27. McInnes IB, and Schett G. 2011 The pathogenesis of rheumatoid arthritis. N Engl J Med 365: 2205–2219. [PubMed: 22150039]

28. Wu EK, Ambrosini RD, Kottmann RM, Ritchlin CT, Schwarz EM, and Rahimi H. 2019 Reinterpreting Evidence of Rheumatoid Arthritis-Associated Interstitial Lung Disease to Understand Etiology. Curr Rheumatol Rev.

29. du Bois R, and King TE Jr. 2007 Challenges in pulmonary fibrosis x 5: the NSIP/UIP debate. Thorax 62: 1008–1012. [PubMed: 17965079]

30. Firestein GS 2003 Evolving concepts of rheumatoid arthritis. Nature 423: 356–361. [PubMed: 12748655]

31. Mateen S, Zafar A, Moin S, Khan AQ, and Zubair S. 2016 Understanding the role of cytokines in the pathogenesis of rheumatoid arthritis. Clin Chim Acta 455: 161–171. [PubMed: 26883280]

32. Keatings VM, O'Connor BJ, Wright LG, Huston DP, Corrigan CJ, and Barnes PJ. 1997 Late response to allergen is associated with increased concentrations of tumor necrosis factor-alpha and IL-5 in induced sputum. J Allergy Clin Immunol 99: 693–698. [PubMed: 9155837]

33. Piguet PF, Ribaux C, Karpuz V, Grau GE, and Kapanci Y. 1993 Expression and localization of tumor necrosis factor-alpha and its mRNA in idiopathic pulmonary fibrosis. Am J Pathol 143: 651–655. [PubMed: 8362967]

34. Libura J, Bettens F, Radkowski A, Tiercy JM, and Piguet PF. 2002 Risk of chemotherapy-induced pulmonary fibrosis is associated with polymorphic tumour necrosis factor-a2 gene. Eur Respir J 19: 912–918. [PubMed: 12030733]

35. Sakao S, Tatsumi K, Igari H, Watanabe R, Shino Y, Shirasawa H, and Kuriyama T. 2002 Association of tumor necrosis factor-alpha gene promoter polymorphism with low attenuation areas on high-resolution CT in patients with COPD. Chest 122: 416–420. [PubMed: 12171811]

36. Dixon WG, Hyrich KL, Watson KD, Lunt M, Consortium BCC, Symmons DP, and British R Society for Rheumatology Biologics. 2010. Influence of anti-TNF therapy on mortality in patients with rheumatoid arthritis-associated interstitial lung disease: results from the British Society for Rheumatology Biologics Register. Ann Rheum Dis 69: 1086–1091. [PubMed: 20444754]

37. Roubille C, and Haraoui B. 2014 Interstitial lung diseases induced or exacerbated by DMARDS and biologic agents in rheumatoid arthritis: a systematic literature review. Semin Arthritis Rheum 43: 613–626. [PubMed: 24231065]

38. Thavarajah K, Wu P, Rhew EJ, Yeldandi AK, and Kamp DW. 2009 Pulmonary complications of tumor necrosis factor-targeted therapy. Respir Med 103: 661–669. [PubMed: 19201589]

39. Nakashita T, Ando K, Kaneko N, Takahashi K, and Motojima S. 2014 Potential risk of TNF inhibitors on the progression of interstitial lung disease in patients with rheumatoid arthritis. BMJ Open 4: e005615.

40. Perez-Alvarez R, Perez-de-Lis M, Diaz-Lagares C, Pego-Reigosa JM, Retamozo S, Bove A, Brito-Zeron P, Bosch X, and Ramos-Casals M. 2011 Interstitial lung disease induced or exacerbated by TNF-targeted therapies: analysis of 122 cases. Semin Arthritis Rheum 41: 256–264. [PubMed: 21277618]

41. Mori S 2015 Management of Rheumatoid Arthritis Patients with Interstitial Lung Disease: Safety of Biological Antirheumatic Drugs and Assessment of Pulmonary Fibrosis. Clin Med Insights Circ Respir Pulm Med 9: 41–49. [PubMed: 26401101]

42. Koo BS, Hong S, Kim YJ, Kim YG, Lee CK, and Yoo B. 2015 Mortality in patients with rheumatoid arthritis-associated interstitial lung disease treated with an anti-tumor necrosis factor agent. Korean J Intern Med 30: 104–109. [PubMed: 25589842]

43. Keffer J, Probert L, Cazlaris H, Georgopoulos S, Kaslaris E, Kioussis D, and Kollias G. 1991 Transgenic mice expressing human tumour necrosis factor: a predictive genetic model of arthritis. EMBO J 10: 4025–4031. [PubMed: 1721867]

44. Li P, and Schwarz EM. 2003 The TNF-alpha transgenic mouse model of inflammatory arthritis. Springer Semin Immunopathol 25: 19–33. [PubMed: 12904889]

45. Li J, Kuzin I, Moshkani S, Proulx ST, Xing L, Skrombolas D, Dunn R, Sanz I, Schwarz EM, and Bottaro A. 2010 Expanded CD23(+)/CD21(hi) B cells in inflamed lymph nodes are associated with the onset of inflammatory-erosive arthritis in TNF-transgenic mice and are targets of anti-CD20 therapy. J Immunol 184: 6142–6150. [PubMed: 20435928]

46. Kuzin II, Kates SL, Ju Y, Zhang L, Rahimi H, Wojciechowski W, Bernstein SH, Burack R, Schwarz EM, and Bottaro A. 2016 Increased numbers of CD23(+) CD21(hi) Bin-like B cells in human reactive and rheumatoid arthritis lymph nodes. Eur J Immunol 46: 1752–1757. [PubMed: 27105894]
47. Douni E, Akassoglou K, Alexopoulou L, Georgopoulos S, Haralambous S, Hill S, Kassiotis G, Kontoyiannis D, Pasparakis M, Plows D, Probert L, and Kollias G. 1995 Transgenic and knockout analyses of the role of TNF in immune regulation and disease pathogenesis. J Inflamm 47: 27–38. [PubMed: 8913927]
48. Proulx ST, Kwok E, You Z, Papuga MO, Beck CA, Shealy DJ, Calvi LM, Ritchlin CT, Awad HA, Boyce BF, Xing L, and Schwarz EM. 2008 Elucidating bone marrow edema and myelopoiesis in murine arthritis using contrast-enhanced magnetic resonance imaging. Arthritis Rheum 58: 2019–2029. [PubMed: 18576355]
49. Bouta EM, Kuzin I, de Mesy Bentley K, Wood RW, Rahimi H, Ji RC, Ritchlin CT, Bottaro A, Xing L, and Schwarz EM. 2017 Brief Report: Treatment of Tumor Necrosis Factor-Transgenic Mice With Anti-Tumor Necrosis Factor Restores Lymphatic Contractions, Repairs Lymphatic Vessels, and May Increase Monocyte/Macrophage Egress. Arthritis Rheumatol 69: 1187–1193. [PubMed: 28118521]
50. Bell RD, Wu EK, Rudmann CA, Forney M, Kaiser CRW, Wood RW, Chakkalakal JV, Paris ND, Klose A, Xiao GQ, Rangel-Moreno J, Garcia-Hernandez ML, Ritchlin CT, Schwarz EM, and Rahimi H. 2019 Selective sexual dimorphism in musculoskeletal-cardiopulmonary pathologies and mortality in the TNF-transgenic mouse model of rheumatoid arthritis. Arthritis & Rheumatology In Press.
51. Rahimi H, Bell R, Bouta EM, Wood RW, Xing L, Ritchlin CT, and Schwarz EM. 2016 Lymphatic imaging to assess rheumatoid flare: mechanistic insights and biomarker potential. Arthritis Res Ther 18: 194. [PubMed: 27586634]
52. Bouta EM, Wood RW, Brown EB, Rahimi H, Ritchlin CT, and Schwarz EM. 2014 In vivo Quantification of Lymph Viscosity and Pressure in Lymphatic Vessels and Draining Lymph Nodes of Arthritic Joints in Mice. J Physiol 592: 1213–1223. [PubMed: 24421350]
53. Bouta EM, Kuzin I, de Mesy Bentley K, Wood RW, Rahimi H, Ji RC, Ritchlin CT, Bottaro A, Xing L, and Schwarz EM. 2017 Treatment of Tumor Necrosis Factor-Transgenic Mice With Anti-Tumor Necrosis Factor Restores Lymphatic Contractions, Repairs Lymphatic Vessels, and May Increase Monocyte/Macrophage Egress. Arthritis Rheumatol In Press.
54. Bouta EM, Ju Y, Rahimi H, de Mesy-Bentley KL, Wood RW, Xing L, and Schwarz EM. 2013 Power Doppler ultrasound phenotyping of expanding versus collapsed popliteal lymph nodes in murine inflammatory arthritis. PLoS One 8: e73766. [PubMed: 24040061]
55. Bell RD, Rudmann C, Wood RW, Schwarz EM, and Rahimi H. 2018 Longitudinal micro-CT as an outcome measure of interstitial lung disease in TNF-transgenic mice. PLoS One 13: e0190678. [PubMed: 29320550]
56. Vande Velde G, Poelmans J, De Langhe E, Hillen A, Vanoirbeek J, Himmelreich U, and Lories RJ. 2016 Longitudinal micro-CT provides biomarkers of lung disease that can be used to assess the effect of therapy in preclinical mouse models, and reveal compensatory changes in lung volume. Dis Model Mech 9: 91–98. [PubMed: 26563390]
57. Misharin AV, Morales-Nebreda L, Mutlu GM, Budinger GR, and Perlman H. 2013 Flow cytometric analysis of macrophages and dendritic cell subsets in the mouse lung. Am J Respir Cell Mol Biol 49: 503–510. [PubMed: 23672262]
58. Guilliams M, Dutertre CA, Scott CL, McGovern N, Sichien D, Chakarov S, Van Gassen S, Chen J, Poidinger M, De Prijck S, Tavernier SJ, Low I, Irac SE, Mattar CN, Sumatoh HR, Low GH, Chung TJ, Chan DK, Tan KK, Hon TL, Fossum E, Bogen B, Choolani M, Chan JK, Larbi A, Luche H, Henri S, Saeys Y, Newell EW, Lambrecht BN, Malissen B, and Ginhoux F. 2016 Unsupervised High-Dimensional Analysis Aligns Dendritic Cells across Tissues and Species. Immunity 45: 669–684. [PubMed: 27637149]
59. Shealy DJ, Wooley PH, Emmell E, Volk A, Rosenberg A, Treacy G, Wagner CL, Mayton L, Griswold DE, and Song XY. 2002 Anti-TNF-alpha antibody allows healing of joint damage in polyarthritic transgenic mice. Arthritis Res 4: R7. [PubMed: 12223110]

60. Proulx ST, Kwok E, You Z, Papuga MO, Beck CA, Shealy DJ, Ritchlin CT, Awad HA, Boyce BF, Xing L, and Schwarz EM. 2007 Longitudinal assessment of synovial, lymph node, and bone volumes in inflammatory arthritis in mice by in vivo magnetic resonance imaging and microfocal computed tomography. Arthritis Rheum 56: 4024–4037. [PubMed: 18050199]
61. Ju Y, Rahimi H, Li J, Wood RW, Xing L, and Schwarz EM. 2012 Validation of 3-dimensional ultrasound versus magnetic resonance imaging quantification of popliteal lymph node volume as a biomarker of erosive inflammatory arthritis in mice. Arthritis Rheum 64: 2048–2050. [PubMed: 22354862]
62. Manzo A, Benaglio F, Vitolo B, Bortolotto C, Zibera F, Todoerti M, Alpini C, Bugatti S, Caporali R, Calliada F, and Montecucco C. 2016 Power Doppler ultrasonographic assessment of the joint-draining lymph node complex in rheumatoid arthritis: a prospective, proof-of-concept study on treatment with tumor necrosis factor inhibitors. Arthritis Res Ther 18: 242. [PubMed: 27770827]
63. Bawadekar M, Gendron-Fitzpatrick A, Rebernick R, Shim D, Warner TF, Nicholas AP, Lundblad LK, Thompson PR, and Shelef MA. 2016 Tumor necrosis factor alpha, citrullination, and peptidylarginine deiminase 4 in lung and joint inflammation. Arthritis Res Ther 18: 173. [PubMed: 27450561]
64. Li J, Zhou Q, Wood RW, Kuzin I, Bottaro A, Ritchlin CT, Xing L, and Schwarz EM. 2011 CD23(+)/CD21(hi) B-cell translocation and ipsilateral lymph node collapse is associated with asymmetric arthritic flare in TNF-Tg mice. Arthritis Res Ther 13: R138. [PubMed: 21884592]
65. Kuzin II, Bouta EM, Schwarz EM, and Bottaro A. 2015 TNF signals are dispensable for the generation of CD23+ CD21/35-high CD1d-high B cells in inflamed lymph nodes. Cell Immunol 296: 133–137. [PubMed: 25959608]
66. Herrinton LJ, Harrold LR, Liu L, Raebel MA, Taharka A, Winthrop KL, Solomon DH, Curtis JR, Lewis JD, and Saag KG. 2013 Association between anti-TNF-alpha therapy and interstitial lung disease. Pharmacoepidemiol Drug Saf 22: 394–402. [PubMed: 23359391]
67. Kim EJ, Elicker BM, Maldonado F, Webb WR, Ryu JH, Van Uden JH, Lee JS, King TE Jr., and Collard HR. 2010 Usual interstitial pneumonia in rheumatoid arthritis-associated interstitial lung disease. Eur Respir J 35: 1322–1328. [PubMed: 19996193]
68. Wolfe F, Caplan L, and Michaud K. 2007 Rheumatoid arthritis treatment and the risk of severe interstitial lung disease. Scand J Rheumatol 36: 172–178. [PubMed: 17657669]
69. Baum S, Schachter O, and Barzilai A. 2016 [PULMONARY FIBROSIS INDUCED BY ANTITNF-Alphalpha TREATMENT]. Harefuah 155: 600–603. [PubMed: 28530055]
70. Fujita M, Shannon JM, Morikawa O, Gauldie J, Hara N, and Mason RJ. 2003 Overexpression of tumor necrosis factor-alpha diminishes pulmonary fibrosis induced by bleomycin or transforming growth factor-beta. Am J Respir Cell Mol Biol 29: 669–676. [PubMed: 12816730]
71. Verrecchia F, Pessah M, Atfi A, and Mauviel A. 2000 Tumor necrosis factor-alpha inhibits transforming growth factor-beta /Smad signaling in human dermal fibroblasts via AP-1 activation. J Biol Chem 275: 30226–30231. [PubMed: 10903323]
72. Yamane K, Ihn H, Asano Y, Jinnin M, and Tamaki K. 2003 Antagonistic effects of TNF-alpha on TGF-beta signaling through down-regulation of TGF-beta receptor type II in human dermal fibroblasts. J Immunol 171: 3855–3862. [PubMed: 14500687]
73. Varga J, and Pasche B. 2008 Antitransforming growth factor-beta therapy in fibrosis: recent progress and implications for systemic sclerosis. Curr Opin Rheumatol 20: 720–728. [PubMed: 18946334]
74. Edwards JCW, Szczepanski L, Szechinski J, Filipowicz-Sosnowska A, Emery P, Close DR, Stevens RM, and Shaw T. 2004 Efficacy of B-cell-targeted therapy with rituximab in patients with rheumatoid arthritis. New Engl J Med 350: 2572–2581. [PubMed: 15201414]
75. Druce KL, Iqbal K, Watson K, Symmons DPM, Hyrich KL, and Kelly C. 2017 Mortality in Patients with Rheumatoid Arthritis and Interstitial Lung Disease Treated with Tumour Necrosis Factor Inhibitor or Rituximab. Rheumatology 56: 127–128.
76. Yusof MYM, Kabia A, Darby M, Lettieri G, Beirne P, Vital EM, Dass S, and Emery P. 2017 Effect of rituximab on the progression of rheumatoid arthritis-related interstitial lung disease: 10 years' experience at a single centre. Rheumatology 56: 1348–1357. [PubMed: 28444364]

77. Hartung W, Maier J, Pfeifer M, and Fleck M. 2012 Effective treatment of rheumatoid arthritis-associated interstitial lung disease by B-cell targeted therapy with rituximab. Case Reports Immunol 2012: 272303. [PubMed: 25379304]

78. Vuillemenot BR, Rodriguez JF, and Hoyle GW. 2004 Lymphoid tissue and emphysema in the lungs of transgenic mice inducibly expressing tumor necrosis factor-alpha. Am J Respir Cell Mol Biol 30: 438–448. [PubMed: 12972399]

79. Sparks JA, He X, Huang J, Fletcher EA, Zaccardelli A, Friedlander HM, Gill RR, Hatabu H, Nishino M, Murphy DJ, Iannaccone CK, Mahmoud TG, Frits ML, Lu B, Rosas IO, Dellaripa PF, Weinblatt ME, Karlson EW, Shadick NA, and Doyle TJ. 2019 Rheumatoid arthritis disease activity predicting incident clinically-apparent RA-associated interstitial lung disease: A prospective cohort study. Arthritis Rheumatol.

80. Lundblad LK, Thompson-Figueroa J, Leclair T, Sullivan MJ, Poynter ME, Irvin CG, and Bates JH. 2005 Tumor necrosis factor-alpha overexpression in lung disease: a single cause behind a complex phenotype. Am J Respir Crit Care Med 171: 1363–1370. [PubMed: 15805183]

81. Miyazaki Y, Araki K, Vesin C, Garcia I, Kapanci Y, Whitsett JA, Piguet PF, and Vassalli P. 1995 Expression of a tumor necrosis factor-alpha transgene in murine lung causes lymphocytic and fibrosing alveolitis. A mouse model of progressive pulmonary fibrosis. J Clin Invest 96: 250–259. [PubMed: 7542280]

82. Thomson EM, Williams A, Yauk CL, and Vincent R. 2012 Overexpression of tumor necrosis factor-alpha in the lungs alters immune response, matrix remodeling, and repair and maintenance pathways. Am J Pathol 180: 1413–1430. [PubMed: 22322299]

Key Points

TNF-Tg mice develop NSIP-like lung disease with increased cDC2 and macrophages

Anti-TNF therapy modulates pre-fibrotic interstitial lung disease in TNF-Tg mice

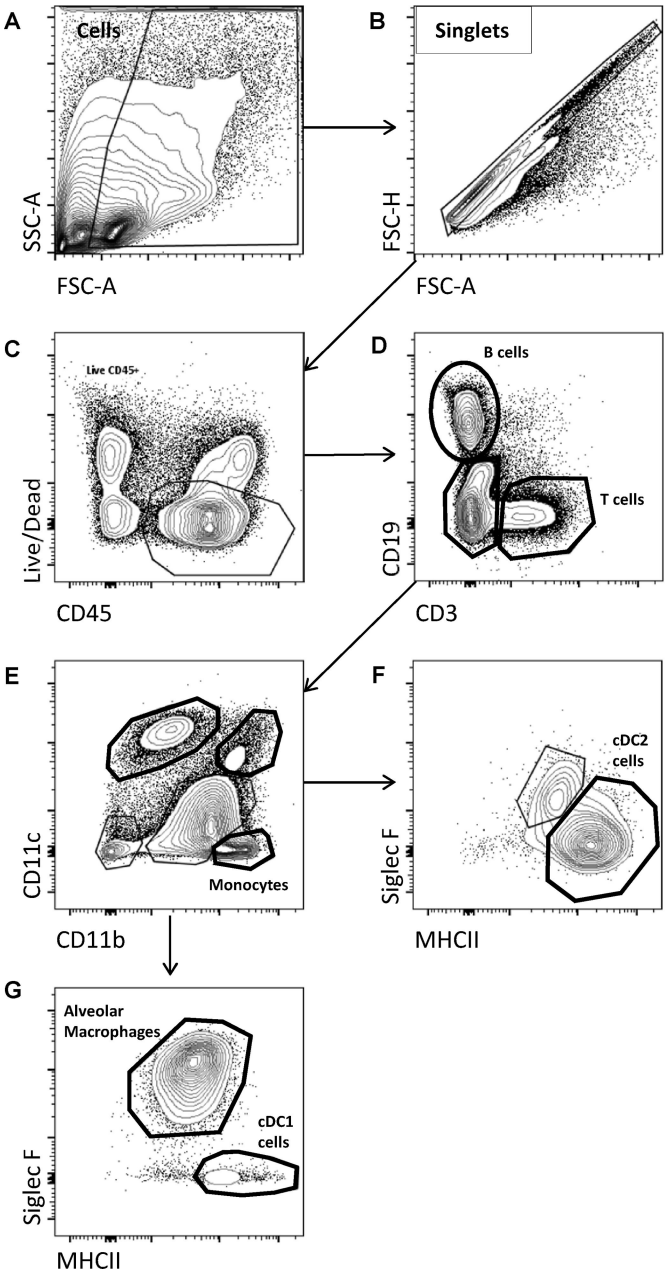

H

	CD11b	CD11c	MHCII	Siglec F	Identity
1	-	++	++	+/-	Alveolar Macs/cDC1
2	++	++	++	-	cDC2
3	++	+	+/-	-	Activated Mono/Mac
4	+	-	-	-	Undiff Mono/Mac
5	-	-	-	-	Unidentified Cells
6	++	-	-	-	Monocytes

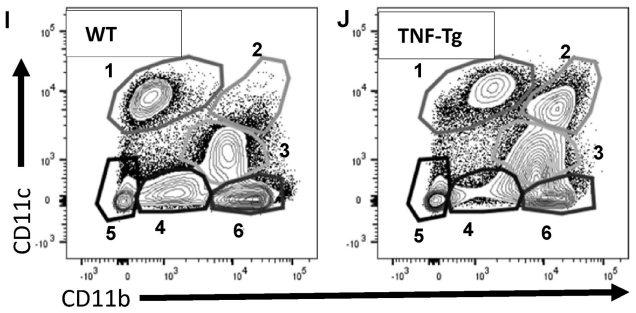

Figure 1. Flow cytometry identifies upregulated myeloid cell populations in TNF-Tg lungs.

Single-cell suspensions of mouse lung digests were analyzed by flow cytometry following fluorescently labeled antibody staining, and analyzed using a sequential gating strategy. After the gating of single cells (A & B), live leukocytes were identified using CD45 and a Live/Dead stain (C). B and T cells were identified with the use of CD19 and CD3 markers (D). From the Live,CD45+CD3-CD19- cells, myeloid populations were analyzed with the use of CD11b, CD11c, MHCII, and Siglec F (E-G). Individual isolated populations were consistent with alveolar macrophages, cDC1s, cDC2s, and monocytes at various stages of activation and transition into macrophages. Population identities with associated marker profiles are listed (H). Representative contour plots for myeloid populations in WT and

TNF-Tg animals demonstrate a difference in profile, specifically regarding populations 2 and 3 (I & J).

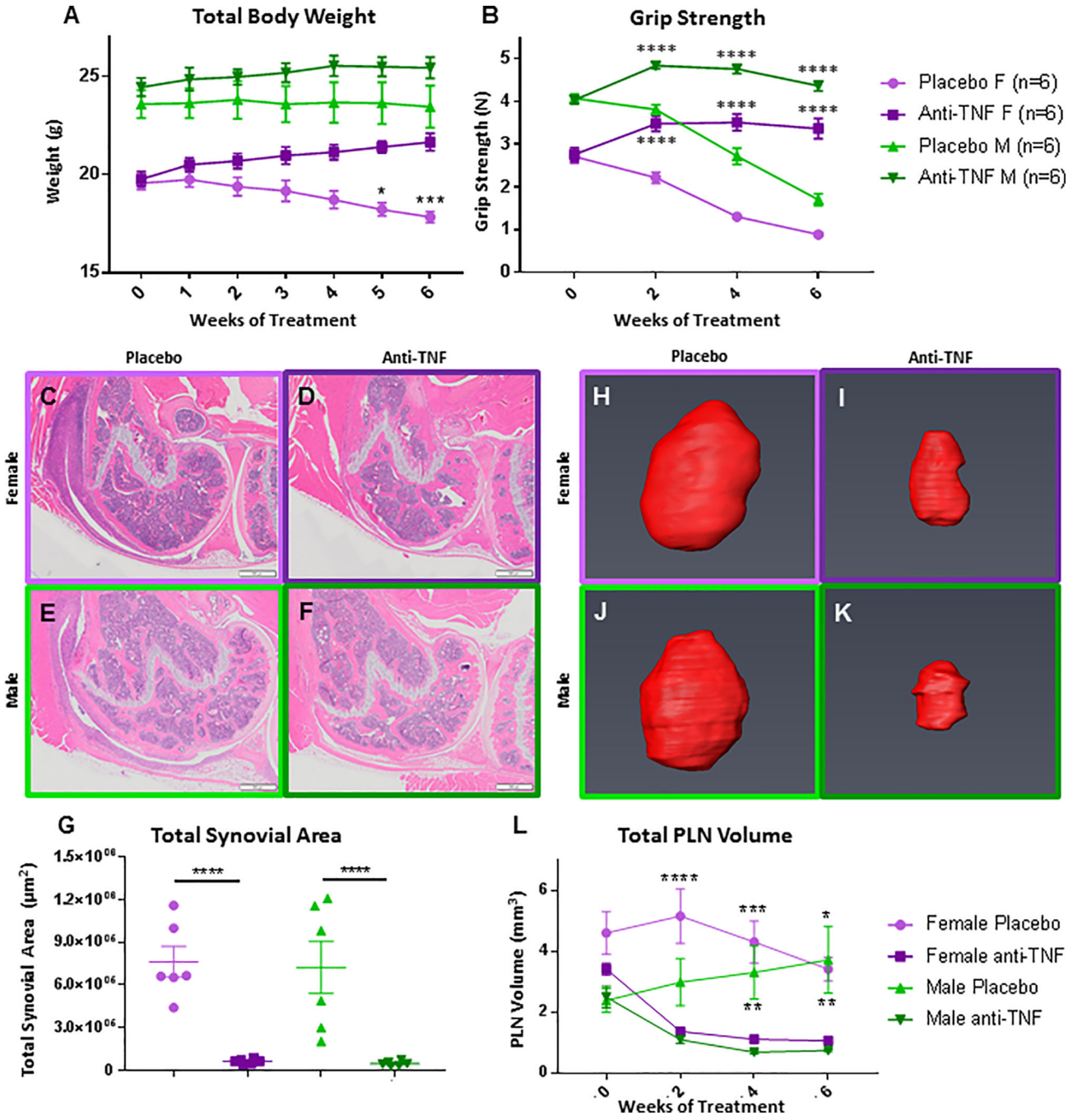

Figure 2. Validation of anti-TNF therapy efficacy.

The effectiveness of the anti-TNF therapy vs. placebo on TNF-Tg treated mice with established inflammatory arthritis described in Supplemental Figure 1 was confirmed by assessing: total body weight (A), grip strength (B), knee synovitis (C-G), and popliteal lymph nodes (E, F) as previously described (Proulx A&R 2007, Bouta A&R 2017). The data are presented as mean ± SEM (Placebo control vs. sex-matched anti-TNF treated cohort, *p<0.05, p**<0.01, p***<0.001, and ****p<0.0001; ɐ Anti-TNF treated males and females, grip strength vs baseline Week 0, p<0.0001).

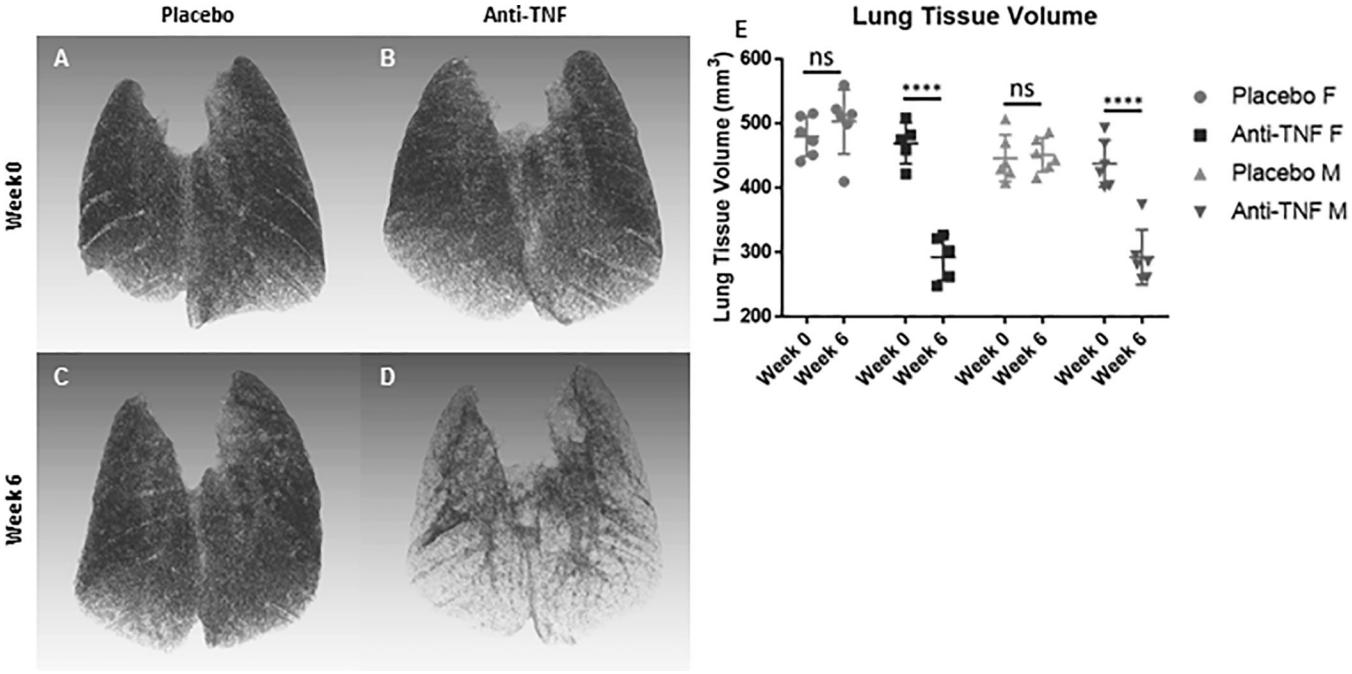

Figure 3. Normal lung tissue volume is recovered in TNF-Tg mice with ILD following anti-TNF therapy.

3D reconstruction of in vivo lung μCT scans described in Supplemental Figure 1 were performed, and representative images of female placebo and anti-TNF treated mice are shown (A-D). Note the marked reduction in tissue volume following 6 weeks of anti-TNF treatment (B vs D). Lung tissue volume from the in vivo mCT scans was quantified prior to (Week 0), and after therapy (Week 6), and the results are presented for each mouse with the mean +/− SD for each group (E, ****$p<0.0001$).

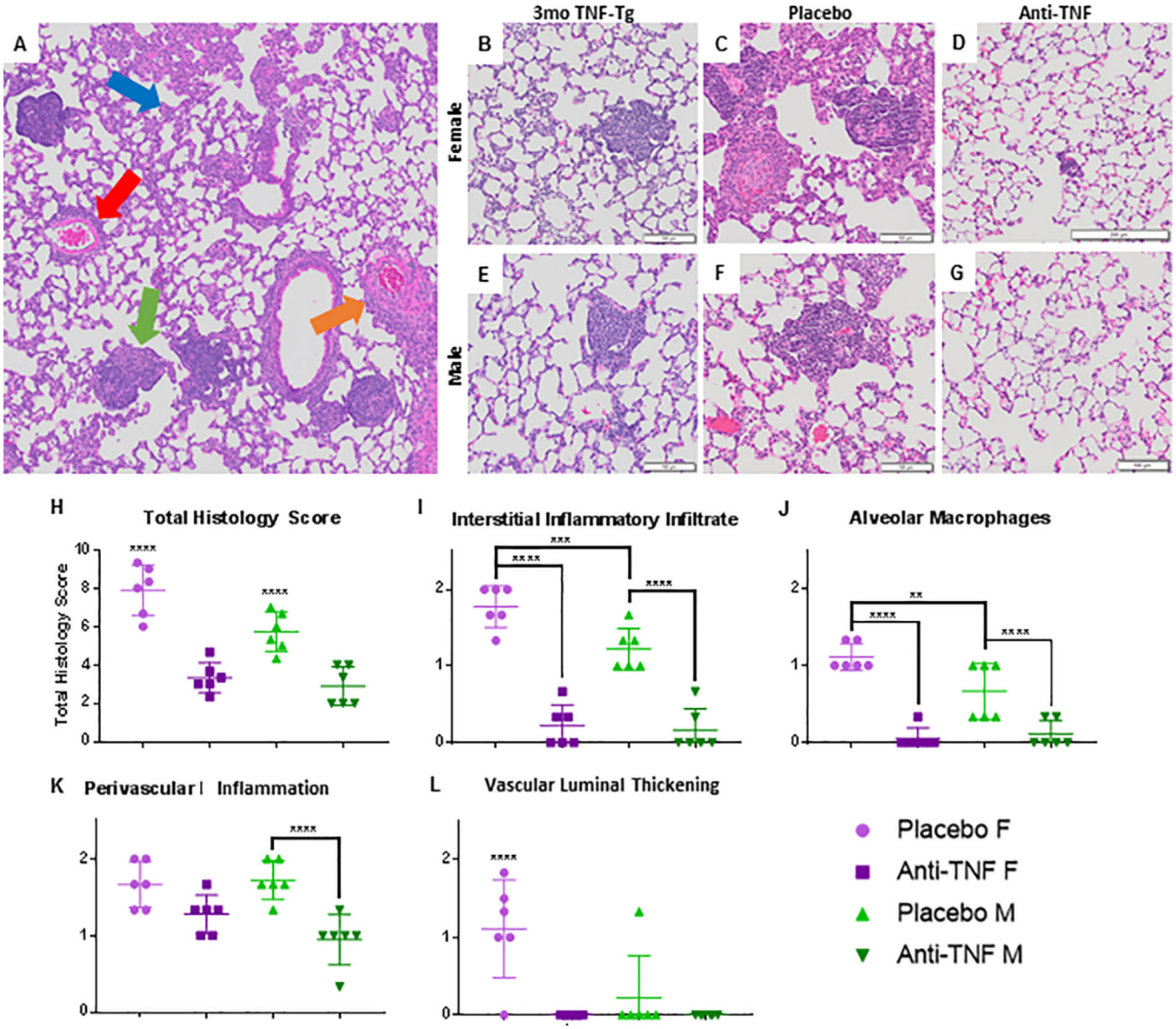

Figure 4. Pulmonary inflammatory infiltrates are ameliorated with anti-TNF therapy.

Lungs from 3-month-old female and male TNF-Tg mice, together with the lungs of the mice described in Supplemental Figure 1, were processed for H&E-stained histology. Representative 8x micrographs are shown with 100mm bar (A-G). Histologic analysis of terminal TNF-Tg lung reveals inflammatory pathology with no interstitial fibrosis (A). The four most notable patterns identified in TNF-Tg lungs include: interstitial cellular infiltration (blue arrow), perivascular inflammation (red arrow), luminal thickening with vascular occlusion (orange arrow), and the formation of follicle-like structures (green arrow). Note that the baseline lung pathology (B, E) progresses during placebo treatment (C, F), and is markedly ameliorated by anti-TNF treatment (D, G). Semiquantitative scoring was performed on the histology, and the data for each treated mouse is presented (mean ± SD for the group, **p<0.01,***p<0.001, ****p=0.0001) (H-L). Note that the severity of interstitial inflammatory infiltrate was significantly decreased with anti-TNF treatment for both sexes

(I), along with alveolar macrophage accumulation (J). Perivascular lymphocytic infiltrates was only decreased in males (K), but arteriolar thickness was decreased in female anti-TNF treated mice. (L).

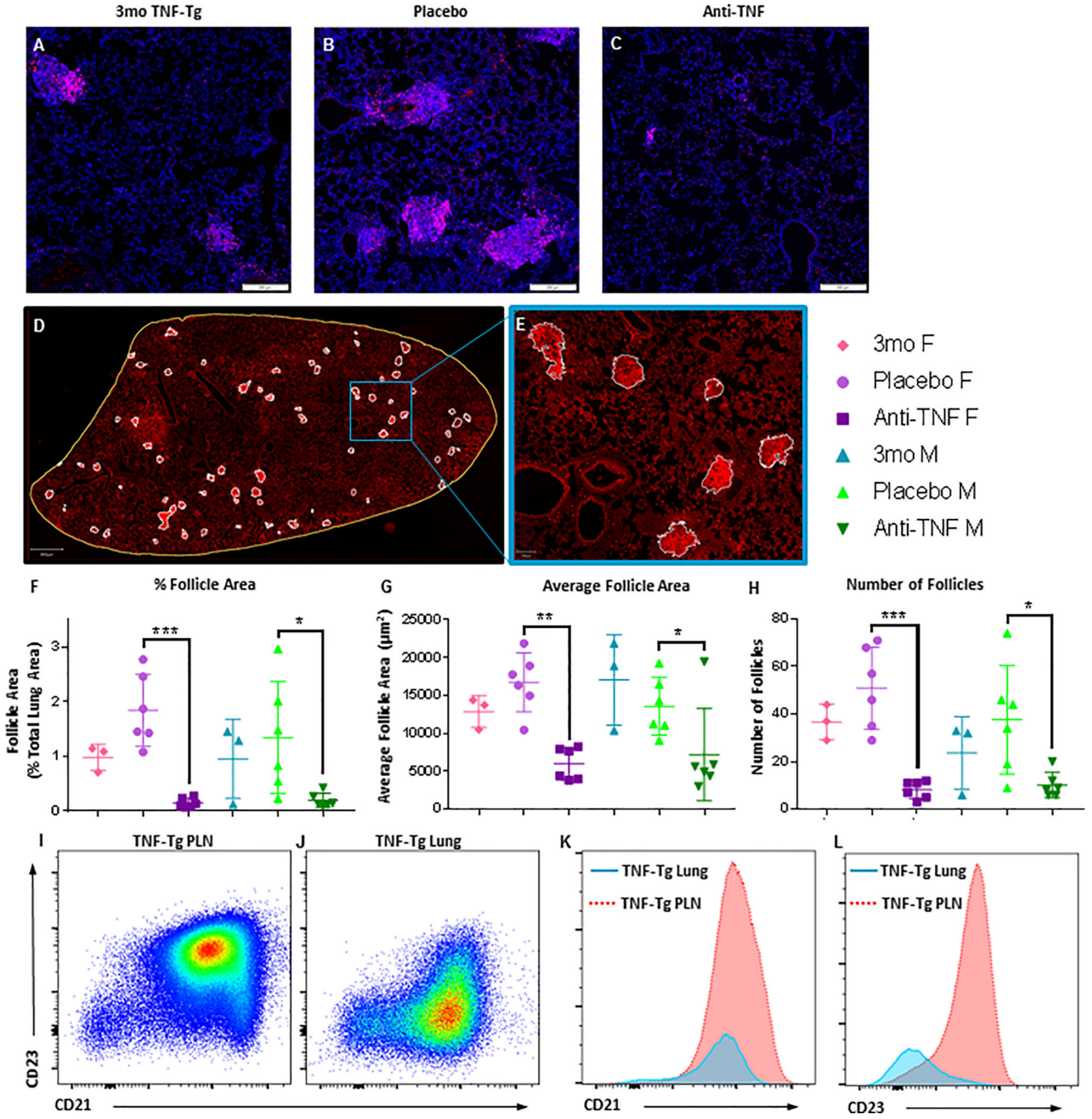

Figure 5. CD21+/CD23- B cell-based follicle-like structures are ameliorated with anti-TNF treatment.

Lungs from all study animals, along with untreated 3-month-old female and male TNF-Tg controls (n=6), were processed for immunohistochemistry and flow cytometry to assess B cell follicles and B cell subsets respectively. Representative 5x micrographs of B220 immunostained lung sections illustrate the increase in B cell follicles in TNF-Tg lungs from 3 to 4.5 months of age, which is ameliorated with anti-TNF therapy (A-C). No sex differences were observed. Semiautomated histomorphometry was performed by manually identifying B220+ follicle-like structures (white outlines), within the total area of the lung

(yellow outline), followed by pixel quantification in QuPath (D). A region of interest (blue box) is shown at 5x-magnification to illustrate the mask method used to identify and quantify the B220+ follicles, based on anatomy and signal intensity (E). From histologic analysis, follicle area (as a percentage of total lung area), average follicle area, and number of follicles per lung are presented (mean ± SD for the group, *$p<0.05$, **$p<0.01$,***$p<0.001$) (F-H). Note that follicle area and total number of follicles was significantly decreased in all anti-TNF treated cohorts when compared to placebo for both sexes. Flow cytometric analysis comparing the known population of CD21hi/CD23+ B cells in popliteal lymph nodes of TNF-Tg mice versus lung B cells in these animals reveals that the B cell-based follicle-like structures are primarily composed of CD21+/CD23- B cells, which are phenotypically distinct from Bin cells (I-L).

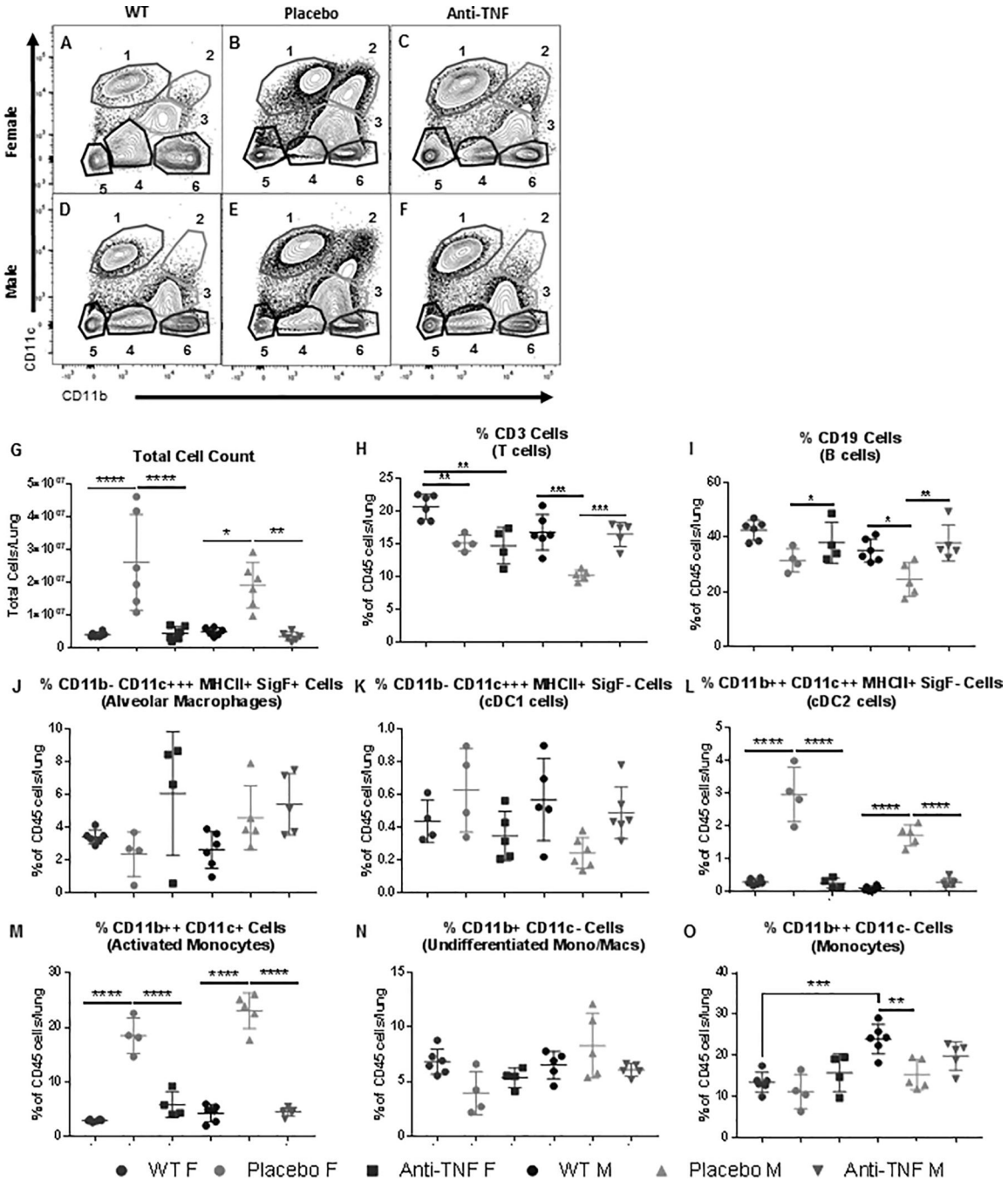

Figure 6. Activated Mono/Mac and cDC2 populations are dramatically increased in lungs with inflammatory infiltrates and revert to a WT-like cellular profile following anti-TNF therapy.

Flow cytometry was performed as described in Figure 4 on lung tissue harvested from the mice described in Supplemental Figure 1 together with untreated WT controls. Representative scatter plots of CD11b and CD11c identify the 6 myeloid cell populations (A-F) detailed in Figure 4H in the lungs of experimental and control cohorts. Total cell counts were decreased to WT levels after anti-TNF treatment for both female and male cohorts (G). Proportionate changes in the cellular profile are most notable in populations 2 and 3, which are most drastically decreased with anti-TNF therapy for both sexes (B vs C;

and E vs F). Quantification of populations as percentages of Live CD45+ cells found significant changes in the cDC2 and activated monocyte populations (H-O, M±SD, *p<0.5, **p<0.01, ***p<0.001).